JACS
JOURNAL OF THE AMERICAN CHEMICAL SOCIETY

Article

pubs.acs.org/JACS

Single-walled Carbon Nanotube Growth from Chiral Carbon Nanorings: Prediction of Chirality and Diameter Influence on Growth Rates

Hai-Bei Li,[†,‡] Alister J. Page,[†,‡] Stephan Irle,*[,§] and Keiji Morokuma*[,‡,∥]

[‡]Fukui Institute for Fundamental Chemistry, Kyoto University, Kyoto 606-8103, Japan

[§]Department of Chemistry, Graduate School of Science, Nagoya University, Nagoya 464-8602, Japan

[∥]Cherry L. Emerson Center for Scientific Computation and Department of Chemistry, Emory University, Atlanta, Georgia 30322, United States

Supporting Information

ABSTRACT: Catalyst-free, chirality-controlled growth of chiral and zigzag single-walled carbon nanotubes (SWCNTs) from organic precursors is demonstrated using quantum chemical simulations. Growth of (4,3), (6,5), (6,1), (10,1) and (8,0) SWCNTs was induced by ethynyl radical (C_2H) addition to organic precursors. These simulations show a strong dependence of the SWCNT growth rate on the chiral angle, θ. The SWCNT diameter however does not influence the SWCNT growth rate under these conditions. This agreement with a previously proposed screw-dislocation-like model of transition metal-catalyzed SWCNT growth rates [Ding, F.; et al. *Proc. Natl. Acad. Sci.* **2009**, *106*, 2506] indicates that the SWCNT growth rate is an intrinsic property of the SWCNT edge itself. Conversely, we predict that the rate of SWCNT growth *via* Diels–Alder cycloaddition of C_2H_2 is strongly influenced by the diameter of the SWCNT. We therefore predict the existence of a maximum growth rate for an optimum diameter/chirality combination at a given C_2H/C_2H_2 ratio. We also find that the ability of a SWCNT to avoid defect formation during growth is an intrinsic quality of the SWCNT edge.

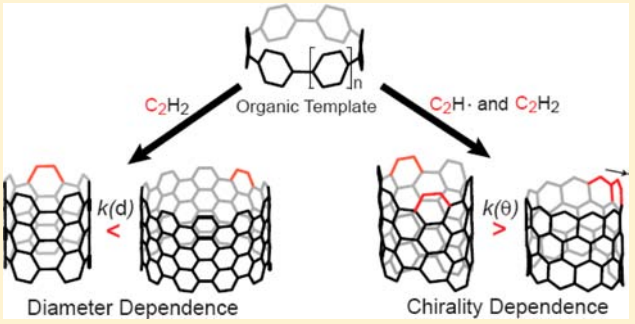

1. INTRODUCTION

Carbon nanotubes (CNTs) exhibit a variety of novel and unique structural, electronic, chemical and mechanical properties.[1−5] The diversity in properties of CNTs, and in particular single-walled CNTs (SWCNTs), depends primarily on their chiral angle,[6] which is conventionally specified by the chiral indices (n,m), which determine the chiral angle, θ. Many of the potential applications of CNTs in various fields are yet to be realized due to the elusiveness of *in situ* control of (n,m) chirality during CNT synthesis.

Traditional CNT growth methods, such as carbon-arc,[7−9] laser evaporation,[10,11] and catalytic chemical vapor deposition (CCVD),[12,13] are incapable of such control, primarily due to the high temperatures employed. In most cases, these temperatures exceed the barrier associated with Stone-Wales transformations, thereby opening up a route by which (n,m) chirality can be lost during growth. Indeed, our own QM/MD simulations[14] of SWCNT growth on transition-metal catalysts show just how chaotic the growth process can be at comparable temperatures. Despite these short-comings, "catalyst-design", and careful control of the experimental conditions constituted the initial attempts toward achieving chirality-controlled CNT growth using such synthetic methods.[15,16] The intervening years however have brought a number of outstanding questions regarding the nature and role of the catalyst during SWCNT growth. For instance, it is still not clear whether the metal catalyst particles maintain highly ordered surface structures during growth or whether they undergo surface melting,[17] restructuring,[18] (sub)surface carbide formation,[19] or carbon-induced step edge formation.[20] Therefore, it seems that catalyst design is in principle an unviable route toward chirality-controlled CNT growth at the present time. Alternatively, postsynthetic isolation of CNTs, *via* methods such as chromatography, polymer-wrapping and density-gradient ultracentrifugation,[21] are effective at producing samples of (n,m) SWCNTs, or at least narrow distributions of different (n,m) SWCNTs. However, such postsynthetic manipulations of SWCNTs are costly and potentially alter or damage the atomic structure of the SWCNTs in the sample. They can therefore only be regarded as a "workaround" for the original synthesis problem. Hence, the goal of *in situ* chirality-controlled CNT growth *via* traditional methods remains outstanding.

A recently proposed bottom-up strategy based upon organic synthetic methods represents a more realistic approach toward chirality-controlled SWCNT growth (the synthesis of which

Received: June 21, 2012
Published: August 28, 2012

   dx.doi.org/10.1021/ja305769v | *J. Am. Chem. Soc.* 2012, 134, 15887−15896

has been reviewed recently in refs 22−26). While the relationship between cycloparaphenylenes (CPP) and the growth of armchair SWCNTs was at first a theoretical hypothesis,[27,28] organic species including CPPs have been synthesized by a number of groups.[29−35] It was originally imagined that chirality-controlled SWCNT growth could be achieved in this manner using low temperature CVD in conjunction with, for example, acetylene. A number of theoretical attempts at understanding this process have since been made. Scott and co-workers[28] proposed that SWCNT growth in this manner is the result of Diels−Alder (DA) cycloadditions *ad infinitum*, with acetylene or related compounds acting as the dieneophile and the growing (*n*,*n*) SWCNT acting as the diene. On the other hand, our own research[36] revealed the potential role of the ethynyl radical, C_2H, on the growth process under low-temperature CVD conditions. Surface catalysis studies[37] have demonstrated that hydrocarbons can be decomposed easily at temperatures as low as 400−500 °C by alumina and silica, producing such radicals. Furthermore, Hung et al.[38] found that C_2H could be formed from the decomposition of C_2H_2 occurring on Fe(100) at temperatures as low as 100 K. Recent QM/MD simulations[39] of acetylene decomposition on Fe nanoparticles have also implicated the C_2H radical as a molecular catalyst for hydrogen disproportionation in hydrocarbon clusters during SWCNT nucleation, that is, C_2H is constantly consumed and recreated. The C_2H radical seems particularly relevant at low temperatures, since the barriers associated with both C−C bond formation and C−H abstraction processes are reduced substantially by the C_2H radical, when compared with traditional DA cycloaddition and subsequent H_2 renormalization reactions.

In the current work, we extend our recent investigation of the role of C_2H in [6]CPP → (6,6) SWCNT growth to a range of chiral (*n*,*m*) SWCNTs and zigzag (*n*,0) SWCNTs using quantum chemical nonequilibrium MD simulations and static density functional theory (DFT) calculations. In this way we will demonstrate for the first time how arbitrary (*n*,*m*) SWCNTs may grow from appropriate chiral and achiral carbon nanorings derived from CPPs[33] at low temperature. We will also establish that, under catalyst-free growth conditions, armchair (or near-armchair) SWCNTs grow faster compared to zigzag (or near-zigzag) SWCNTs. While such a chirality-relationship has been proposed previously in the context of transition-metal catalyzed growth in a model known as "screw-dislocation-like" (SDL) growth,[40] we will show that this relationship holds during radical addition reactions in actual nonequilibrium MD simulations. We will also address the issue of diameter dependence of SWCNT growth rates under conditions of radical C_2H insertion and C_2H_2 Diels−Alder cycloaddition, showing in particular a strong relationship between SWCNT growth rate and the SWCNT diameter, *d*, in the latter case.

2. COMPUTATIONAL DETAILS

The computational methodology employed in this work is the same as that used by us in our recent investigation of [6]CPP → (6,6) SWCNT growth.[36] Chirality-controlled growth of (4,3), (6,5), (6,1), (10,1) and (8,0) SWCNTs was achieved by the periodic addition of C_2H radicals to [2]CPPN, [4]CPPN, [0]CPPH, [0]CPPD and cyclooctacene precursors (Figure 1), respectively. Here we employ the [*n*]CPPx nomenclature of Omachi et al.,[33] where *x* = N, H and D denotes napthylene, hexylene and decylene, respectively. As shown in Figure 1, these SWCNTs provide a range of both *d* and *θ*. After the

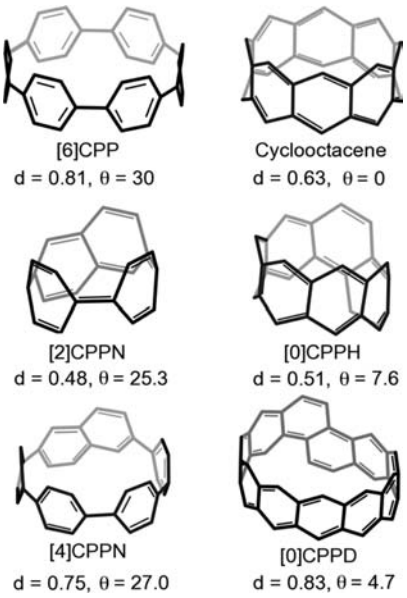

Figure 1. Organic templates for SWCNT growth simulations. [6]CPP, cyclooctacene, [2]CPPN, [0]CPPH, [4]CPPN and [0]CPPD precursors ultimately become (6,6), (8,0), (4,3), (6,1), (6,5) and (10,1) SWCNT fragments, respectively. Diameters *d* and chiral angles *θ* are given in nm and degrees, respectively.

geometries of these model systems were optimized, the model systems were equilibrated at 500 K for a period of 5 ps. SWCNT growth was then induced by the addition of one C_2H radical to a randomly chosen carbon atom in the SWCNT fragment at regular intervals of 10 ps. This rate is, in a sense, somewhat arbitrary. However, not only are higher C_2H supply rates expected to increase defect formation during growth, they are also unrealistic considering the anticipated fraction of C_2H present in experimental growth conditions. The center of mass of the incoming C_2H radical was positioned randomly between 3 and 4 Å from the target carbon atom, along the vector joining the target atom and the center of mass of the C_2H radical. The initial velocity of each incoming atom coincided with the nuclear temperature of the entire system (500 K); however, drawing velocities from a Boltzmann distribution at an equivalent temperature has been shown to have no effect on the outcome of the simulation. Full details of this supply algorithm have been described elsewhere.[41,42] The formation of new hexagonal rings is an infrequent event, and so a "selective" MD method, reminiscent of Voter's parallel replica MD method,[43] was employed. Initially, six independent SWCNT growth trajectories were generated. After each consecutive 10 ps period of QM/MD simulation, the two trajectories that were judged to most favor the growth of SWCNTs were selected as the next set of initial structures for the subsequent period of simulation. The criterion employed as the measure of growth was hexagon formation, following a thermodynamic stability argument.[44] Each of these structures was then replicated six times, and so on. These QM/MD growth trajectories therefore gave rise to an exponentially branching "trajectory-tree" structure. For the purposes of analysis and discussion however, we limit our analysis to a single "branch" (consisting of 6 trajectories) of the trajectory-tree. As we have recently established,[36] the abstraction of hydrogen from [6]CPP/(6,6)SWCNT was extremely easy with a barrier of only 1−2 kcal/mol. Interaction of C_2H with [6]CPP/(6,6) SWCNT results in the abstraction of a [6]CPP/(6,6) SWCNT hydrogen approximately 40% of the time, thereby facilitating SWCNT growth *via* hexagon formation. Two hydrogen atoms were therefore removed from the growing SWCNTs every 20 ps during the initial period of growth in this work in order to increase the efficiency of the growth simulations. Supplementary QM/MD simulations have established that this hydrogen removal scheme does not adversely affect the mechanism of SWCNT growth.[36] While this is in some sense

dx.doi.org/10.1021/ja305769v | J. Am. Chem. Soc. 2012, 134, 15887−15896

artificial, hydrogens were removed from all SWCNTs at comparable rates; for (6,5)/(10,1) SWCNTs and (4,3)/(6,1) SWCNTs, 20 and 10 hydrogen atoms were removed, respectively. The ratios of edge hydrogens in the corresponding organic precursors to that removed were therefore 1:1.1 and 1:1.4, respectively. For (8,0) SWCNTs 28 hydrogen atoms were removed in total, giving a ratio of 1:1.67 (while this is a larger ratio, this is irrelevant considering the nature of (8,0) SWCNT growth as we show below).

All QM/MD simulations employed the self-consistent charge density-functional tight-binding (DFTB) method.[45] DFTB is an approximate density functional theory (DFT) method based on the tight binding approach and is at least 2 orders of magnitude faster than DFT method for systems of this nature, while providing remarkably similar energetics and structures.[46,47] The DFTB wave function, energy and gradient were computed "on-the-fly" at each MD step. A finite electronic temperature (T_e)[48,49] of 1500 K was enforced on the DFTB wave function. Orbital occupations were therefore described by a Fermi-Dirac distribution, and varied continuously between [0,2] near the Fermi level. The Newtonian equations of motion were integrated using the popular Velocity-Verlet algorithm.[50] In periods between consecutive C_2H additions/hydrogen removal, the *NVT* ensemble was enforced on all systems *via* a Nosé-Hoover chain thermostat (chain length = 3).[51] The nuclear temperature was maintained at 500 K throughout all simulations.

Further analysis of the SWCNT growth trajectories has been made using the (U)B3LYP[52,53] functional of density functional theory, in conjunction with the 6-31G(d) basis set. While this combination of functional and basis set is not perfect in the context of large polycyclic aromatic hydrocarbon systems, it allows direct comparison with several recent calculations concerning SWCNT growth.[28,36] All B3LYP/6-31G(d) calculations were performed using the Gaussian09 program.[54] Frequency calculations were carried out to ensure that true local minima and transition states (TS) were located. The intrinsic reaction coordinate method[55] was also performed to ensure that a TS connects two appropriate local minima in the reaction pathway. For all stationary points located, harmonic zero-point vibrational energies and thermal corrections at 500 K were taken into account.

3. RESULTS: QM/MD SIMULATIONS OF CHIRALITY-CONTROLLED SWCNT GROWTH

3.1. Armchair SWCNT Growth. We begin initially by briefly reiterating the main conclusions of our recent investigation of [6]CPP → (6,6) SWCNT growth,[36] since much of the subsequent discussion is concerned with the impact of d and θ on the mechanism and rate of SWCNT growth. These previous quantum chemical simulations demonstrated the dual role of the C_2H radical during SWCNT under the current conditions, that is, it is both the initiator of SWCNT growth (*via* hydrogen abstraction) and the agent of SWCNT growth itself. SWCNT growth from the [6]CPP precursor proceeded essentially *via* the formation of extended polyyne chains at the edge of the SWCNT fragment. Ultimately, following 485 ps of QM/MD growth simulation, the [6]CPP had been converted into a (6,6) SWCNT *ca.* 7.5 Å in length following the addition of 27 new hexagons. The energetics of growth was extremely competitive in comparison to a DA-based growth mechanism. For example, the barrier ($\Delta G^{\ddagger}$(500 K)) associated with hydrogen abstraction was essentially nonexistent. Similarly, $\Delta G^{\ddagger}$(500 K) corresponding to the formation of hexagons and pentagon defect structures were *ca.* 20−40 and 2−56 kcal/mol, respectively, depending on the hydrogen concentration at the precursor edge. Moreover, the prior interaction of the C_2H radical and the SWCNT significantly enhanced the energetics of SWCNT growth *via* acetylene addition. For instance, the prior abstraction of a single hydrogen at the [6]CPP "bay" region by C_2H gives a $\Delta G^{\ddagger}$(500 K) value of *ca.* 6 kcal/mol; the prior abstraction of both hydrogens resulting in acetylene is barrierless. For comparison, DA addition of acetylene in this case requires a $\Delta G^{\ddagger}$(500 K) of *ca.* 53 kcal/mol (with hydrogen abstraction to follow).

3.2. Chiral SWCNT Growth. The evolution of (6,5) and (10,1) SWCNT growth is depicted in Figure 2 and Movie S1 in Supporting Information. Analogous structures of (4,3) and (6,1) SWCNTs (which have approximately the same angle θ but different diameter d) are provided in Supporting Information (Figure S1).

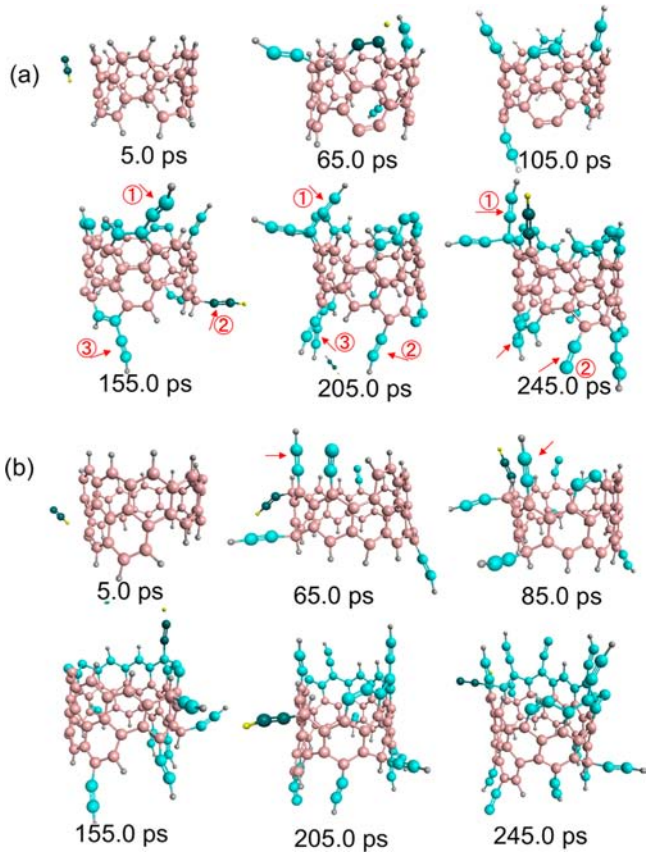

Figure 2. Evolution of (a) [4]CPPN→ (6,5) SWCNT and (b) [0]CPPD → (10,1) SWCNT growth. Gray, hydrogen; pink, carbon in the organic precursor; cyan, previously added C_2H radicals; dark green, most recently added C_2H radical.

Regarding both near-armchair and -zigzag SWCNT growth, two primary roles of the C_2H radicals were observed during these QM/MD simulations, viz. hydrogen abstraction and C_2H radical addition to the precursor. The latter of these drove SWCNT growth itself. This behavior is unsurprising, having been shown also in our previous investigation.[36] Armchair edge carbon atoms of the organic precursor served as "docking points" for the incoming C_2H radicals (Scheme 1a). We note here that new hexagon formation always occurred at an armchair "bay"-region, irrespective of the precise (n,m) chirality of the whole SWCNT. Presumably then the energetics of C_2H-based SWCNT growth of near-armchair and -zigzag SWCNT is similar to those in the case of armchair SWCNTs, which have already been established.[36] We will return to the ramifications of this observation in the context of SWCNT growth rates in the Discussion. Following 105 ps, two hexagons (at random

dx.doi.org/10.1021/ja305769v | J. Am. Chem. Soc. 2012, 134, 15887−15896

Scheme 1. Schematic Depiction of C_2H-based SWCNT Growth from Organic Precursors[a]

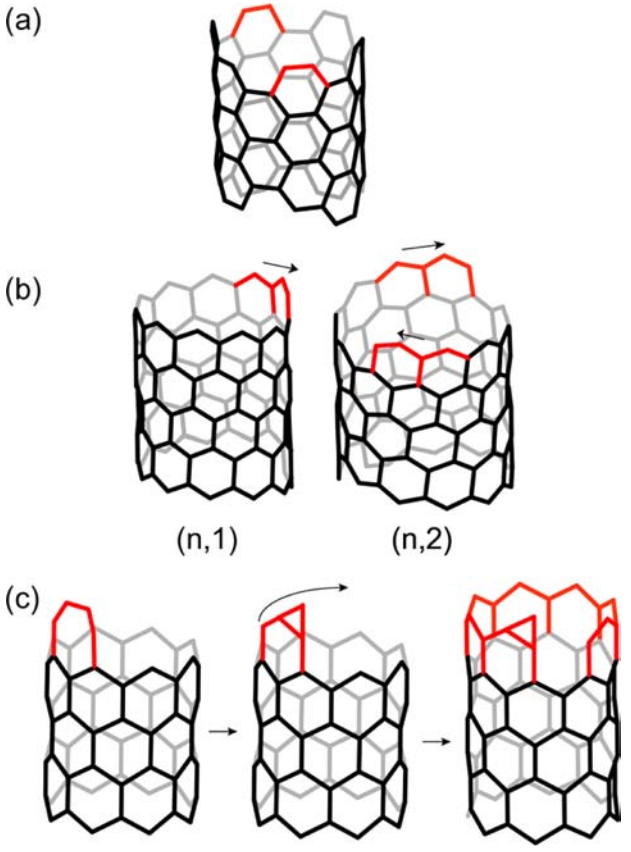

[a]Such growth is typified as either (a) random/non-sequential (armchair/near-armchair $(n,n) - (n,n/2)$ SWCNTs), (b) sequential (near-zigzag $((n,1) - (n,(n/2)\text{-}1)$ SWCNTs) or (c) "terminal" (zigzag $(n,0)$ SWCNTs) in nature. Zigzag growth is both initiated and ultimately prevented by the presence of a 6-3 defects at the growing SWCNT edge.

armchair sites) were formed in the case of (6,5) SWCNT growth, and another four C_2 chains were attached to the precursor (Figure 2a). In the subsequent 50 ps, isomerization of these chains yielded an additional four new hexagons. In all cases, hexagons resulted from the free motion of the carbon chains. As was the case for [6]CPP → (6,6) SWCNT growth, hexagon formation here was impeded significantly by the presence of terminating hydrogen atoms on the precursor; hexagon formation was typically observed following the abstraction of such hydrogens. Such seemingly random addition of hexagons during growth is typical of armchair or near-armchair SWCNT growth. Such addition also led to the existence of zigzag edge "substructures" in the growing SWCNT structure. In the case of (6,5) SWCNT growth, three such substructures existed at 155 ps, constituting a total of eight "zigzag" carbon atoms (denoted by arrows and labels, Figure 2a).

Near-zigzag SWCNT growth (depicted in Figure 2b), typified by the (10,1) SWCNT case, exhibited fundamental differences compared to (6,5) SWCNT growth. The pristine [0]CPPD precursor in this case initially possessed a single armchair position on both edges. As was the case with armchair or near-armchair SWCNT growth, discussed above, growth in the case of near-zigzag SWCNTs corresponded to hexagon addition *only* at these armchair edge structures. While such addition in the case of armchair/near-armchair SWCNTs led to the formation of zigzag edge structures at the expense of amchair edge structures, the situation is reversed in the case of near-zigzag growth. That is, no armchair edge structure is destroyed during growth; it is simply shifted one position along the edge of the growing SWCNT structure in a sequential manner akin to the SDL model of Ding et al.[40] This process is shown clearly in Figure 2b between 65 and 155 ps; during this period six new hexagons are formed by such sequential growth (denoted with arrows, Figure 2b). The passivating effects of hydrogen on the dynamics of these adsorbed chains are also illustrated in Figure 2b. For example, on the other edge of the growing SWCNT at 245 ps there are in total five C_2H and a single C_2 chain adsorbed on the SWCNT. However, since the single armchair carbon is terminated by hydrogen, the addition of the first hexagon, and hence all subsequent hexagons, is prevented. Presumably this shortcoming of sequential hexagon addition, which typifies the growth of near-zigzag SWCNTs, impedes the SWCNT growth rate in comparison to armchair/near-armchair SWNCTs. This point will be expanded upon in the Discussion.

We have established that hexagon-only SWCNT growth ultimately equates to C_2 addition at the armchair edge structure, regardless of the (n,m) chiral indices of the growing SWCNTs. Yet in the case of zigzag $(n,0)$ SWCNTs, no such edge structures exist. What then is the mechanism of growth in this case?

3.3. Zigzag SWCNT Growth. QM/MD simulation of (8,0) SWCNT growth is depicted in Figure 3a. During the initial stages of growth, the actions of incoming C_2H radicals were more limited compared to chiral and armchair SWCNT species. Either these radicals abstracted terminal hydrogen atoms from the growing SWCNT, or they inserted directly at the SWCNT edge. Several examples of the latter phenomenon are evident in Figure 3a. The first polygonal carbon ring formed in this trajectory was a defect heptagon (67.4 ps). This defect ultimately proved to be unstable, yielding instead a conjugated benzocyclopropene radical at the edge of the cyclooctacene precursor. The latter evidently exhibited greater structural stability compared to the heptagon defect at 500 K. Indeed, Figure 3a shows that such "6−3" conjugated ring structures are prominent throughout (8,0) SWCNT growth. By undergoing this isomerization, what was originally a defect in fact promotes chirality-controlled growth, *via* the formation of a new armchair site at the growing (8,0) SWCNT edge. As one may expect, the manner in which the (8,0) SWCNT was subsequently extended resembled that of near-zigzag SWCNTs, discussed above. That is, SWCNT growth was driven by the repeated addition of hexagons from this armchair edge structure. We note here however that this extension was not sequential, as in the case of (10,1) and (6,1) SWCNTs discussed above, since the numbers of armchair edge structures were subject to change. For example, Figure 3a shows that at 115 ps only one such 6−3 structure existed, while 130 ps later no fewer than three such structures existed. By 325 ps, a total of eight new hexagons had been added to the precursor, and yet neither edge had been extended "completely". The single impediment to the formation of a complete row of new hexagons was, ironically, the same structural feature that enabled hexagon addition in the first place, the 6−3 conjugated ring structure (Figure 3b). The three-membered ring proved so stable that no 6−3 → 6−6 ring isomerization was observed within 325 ps. Using DFT this

dx.doi.org/10.1021/ja305769v | J. Am. Chem. Soc. 2012, 134, 15887−15896

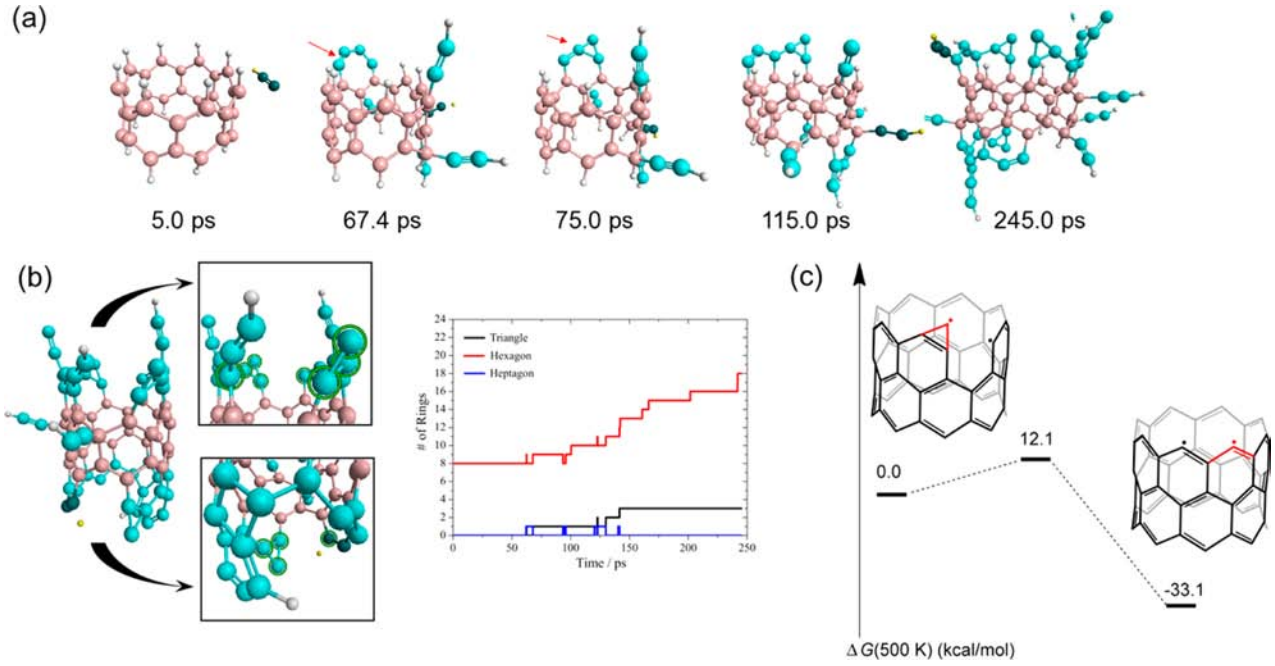

Figure 3. (a) Evolution of cyclooctacene → (8,0) SWCNT growth using C_2H radicals at 500 K. (b) Structure obtained at 325 ps; complete extension of the hexagonal lattice is not observed in QM/MD simulations at 500 K, and is prevented by 6−3 defect structures at the SWCNT edge. Gray spheres represent hydrogen; pink spheres represent carbon in the cyclooctacene precursor, cyan spheres previously added C_2H radicals, dark spheres the most recently added C_2H radical. (c) In the absence of terminating hydrogen, the 6−3 → 6−6 ring isomerization is exothermic and corresponds to a $\Delta G^{\ddagger}$(500 K) of *ca.* 12.1 kcal/mol using B3LYP/6-31G(d).

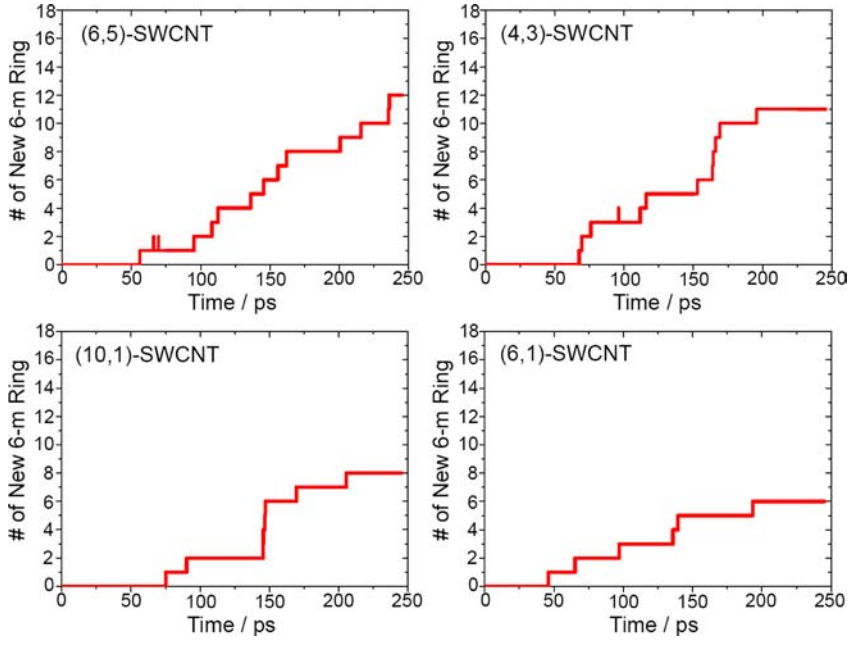

Figure 4. Hexagon formation observed during (6,5), (10,1), (4,3), and (6,1) SWCNT growth.

barrier corresponded to $\Delta G^{\ddagger}$(500 K) of only 12.1 kcal/mol, somewhat surprisingly, and was exothermic by 33.1 kcal/mol (in the presence of hydrogen termination, this same reaction is strongly exothermic by 50.3 kcal/mol). Thus, although highly exothermic, our QM/MD simulations suggest that this 6−3 defect is kinetically stable.

This 6−3 → 6−6 ring isomerization is akin to the "reinitiation" step in Ding et al.'s SDL picture of SWCNT growth.[40] The crucial difference, however, is that screw-dislocation reinitiation concerns the free energy associated with the emergence of a *new* layer in the zigzag SWCNT, while we show here a *barrier* corresponding to the completion of the *current* layer. The two processes are significantly different in an energetic sense; compared with 12 kcal/mol for 6−3 → 6−6 ring isomerization, DFT reinitiation energies on Fe, Co and Ni catalysts range from 25 to 35 kcal/mol.[40] Moreover, Figure 3 shows that, in this case, reinitiation of the subsequent layer of the (8,0) SWCNT is not the rate-limiting step during growth. However, without 6−3 → 6−6 ring isomerization, and thus the complete extension of the hexagonal lattice, SWCNT growth is

dx.doi.org/10.1021/ja305769v | J. Am. Chem. Soc. 2012, 134, 15887−15896

effectively terminated. Experimental distributions of (*n*,*m*) SWCNT abundances show a distinct lack of zigzag, or near-zigzag SWCNTs, suggesting growth of such SWCNTs is less favorable.[15,56] To equate the results of our simulations and such experimental observations is specious in a sense, since we are concerned with low-temperature, catalyst-free SWCNT growth. However, we believe that both results are manifestations of the underlying difficulties inherent during the growth of zigzag SWCNTs.

4. DISCUSSION

4.1. Dependence of SWCNT Growth Rate on Chiral Angle. As discussed in the preceding section, the growth of armchair/near-armchair SWCNTs from organic precursors is significantly different from that of near-zigzag SWCNTs. Hexagon addition in the case of the former occurs at essentially random armchair sites, whereas hexagon addition in the case of the latter is much more sequential in nature. This sequential near-zigzag growth arises from the single, domineering armchair site on the growth SWCNT edge in the latter case. On the other hand, the growth of zigzag SWCNTs is kinetically unfavorable. We now turn to a more detailed discussion of the relationship between the chiral angle θ of the SWCNT and the SWCNT growth rate.

SWCNT growth rate can be interpreted most accurately in this context by the rate of hexagon addition. Figure 4 presents the statistics of new hexagonal ring formation during the SWCNTs growth process for both near-armchair and near-zigzag SWCNTs after 245 ps. For the near-armchair (6,5) and (4,3) SWCNTs, 12 and 11 hexagons were added during this period, respectively, while for the near-zigzag (10,1) and (6,1) SWCNTs only eight and six were added. For comparison, the number of hexagons added during (6,6) SWCNT growth from [6]CPP[36] during the same period was 11. This data suggests immediately that hexagon addition is more favored during growth of near-armchair SWCNTs, compared to near-zigzag SWCNTs. The underlying reason is obvious; in the case of an armchair SWCNT, all incoming C_2H are positioned at such armchair positions, and thus all C_2H (or more generally C_n chains) may potentially form new hexagons. The number of such sites in a near-armchair SWCNT is only slightly diminished, thereby furnishing a comparable growth rate. In the case of near-zigzag SWCNTs, few armchair sites exist, which forces 'sequential' growth of the SWCNT fragment at a substantially slower rate. And as we have established above, the situation is worst in the case of zigzag SWCNT fragments. Thus, the growth rate of a SWCNT in the absence of a catalyst is directly proportional to the chiral angle θ of that SWCNT. This result is in line with a number of previous investigations concerning transition-metal catalyzed SWCNT growth, such as the SDL growth model.[40,57,58] However, in the absence of a catalyst, the simulations presented here confirm that this relationship is an intrinsic property of a SWCNT edge itself. While such an intrinsic relationship has been shown previously for graphene edges,[57] the results here are the first *in situ* demonstration of such a relationship in SWCNT growth.

A distinct relationship between the chiral angle θ and the rate of defect formation was also observed in these simulations. It is immediate from Figure 5 that fewer defects (classified as four-, five- and seven-membered rings) form during growth of near-armchair SWCNTs compared to growth of near-zigzag SWCNTs. This is particularly the case during the earliest stages of growth, when the SWCNT fragment most resembles its organic precursor. For example, for the (10,1) SWCNT growth trajectory, on two separate occasions only one of six trajectories *did not* form a defect (between 50 and 60 and 140–150 ps). This is also the case, albeit to a less dramatic extent, for the (6,1) SWCNT growth trajectory. On the other hand, growth of the (4,3) and (6,5) SWCNT fragments during this period is relatively "defect-free". Admittedly, however, the number of defects in the case of (6,5) SWCNT formed between 230 and 240 ps is more noticeable, and is due to a larger concentration of polyyne chains attached to the growing SWCNT fragment at this time. These observations are consistent with those previously made during QM/MD simulations of SWCNT growth on Fe_{38} catalyst nanoparticles.[59] In this latter investigation, it was reported that (5,5) SWCNTs have a greater averseness to defect formation, compared to (8,0) SWCNTs. This averseness is also consistent with the relative "edge energies"[57] of near-armchair and near-zigzag graphene edges in vacuum. The observation of this trend in the absence of a catalyst indicates that the ability to avoid defect formation is also an intrinsic property of the SWCNT structure itself. That is, it does not originate from the interaction between the SWCNT and a supporting catalyst nanoparticle. Thus, by varying the strength of the SWCNT-catalyst interactions (i.e., catalyst-design approaches to chirality control), one can presumably only mitigate or enhance this trend, not reverse it completely.

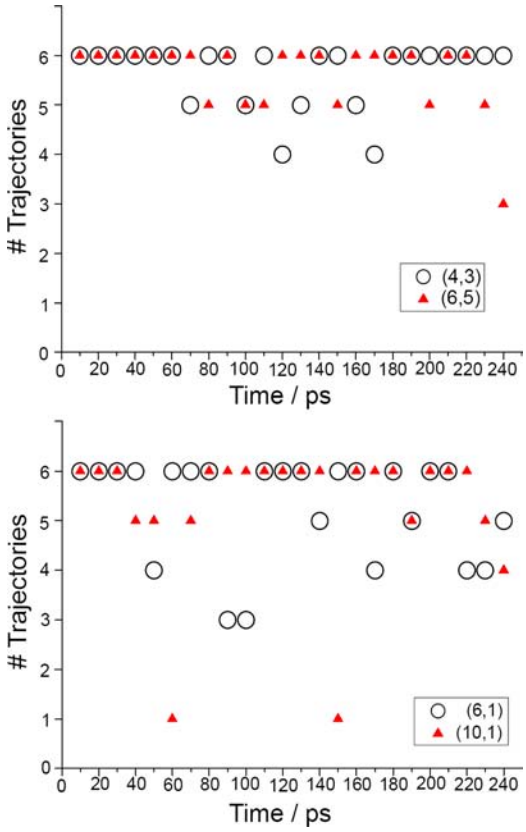

Figure 5. Numbers of "successful" QM/MD simulations of (a) near-armchair and (b) near-zigzag SWCNT growth. Success is defined as the total absence of any defects (i.e., four-, five- and seven-membered rings) during each simulation period, that is, chirality-controlled growth. In the absence of a catalyst, near-armchair SWCNTs exhibit a greater tendency toward maintaining their chirality compared to near-zigzag SWCNTs.

dx.doi.org/10.1021/ja305769v | J. Am. Chem. Soc. 2012, 134, 15887–15896

4.2. Dependence of SWCNT Growth Rate on Diameter. Thus far we have confirmed by nonequilibrium MD simulations that SWCNT growth rates from organic precursors are proportional to the chiral angle θ of the growing SWCNTs. We now consider the dependence of SWCNT growth rate on the SWCNT diameter. Despite a number of detailed previous theoretical investigations of SWCNT growth from organic precursors in the literature,[27,28,36] the relationship between growth dynamics and SWCNT diameter remains unaddressed. Peng et al.[60] have previously shown that a SWCNT's stability depends strongly on its diameter, with smaller diameter SWCNTs being intrinsically higher in energy compared to larger diameter SWCNTs due to their higher curvature. This would seemingly suggest that larger diameter SWCNTs exhibit higher growth rates, since the decreased sp^2 curvature may enhance the energetics of the hexagon formation process. This is indeed true, in particular cases, as we discuss below. Nevertheless, diameter-independence is implicit in current models of transition-metal catalyzed SWCNT growth.[40] Figure 4 shows that in the case of SWCNT growth from [*n*]CPP *via* C_2H insertion, the growth rate is also independent of the SWCNT diameter. For both small diameter ((4,3), (6,1)) and large diameter ((6,5), (10,1)) SWCNTs, hexagons are added at approximately the same rate. Therefore, independence of SWCNT growth rates on SWCNT diameter under such conditions is also an intrinsic quality of the SWCNT structure.

The energetics of SWCNT growth *via* C_2H radical insertion and its dependence on SWCNT diameter have been modeled using [*n*]CPP precursors (Figure 6a). In this case hexagon formation results from a simple isomerization of the inserted C_2H radical at an armchair edge structure, and is only favorable in the absence of both terminating hydrogens.[36] Figure 6b shows that the barrier preventing hexagon addition *via* C_2H insertion decreases only slightly with increasing SWCNT diameter, and is thus in agreement with the diameter-independent growth rates obtained from QM/MD simulation. Regarding the exothermicity of the isomerization process, the trend is more noticeable, that is, the reaction becomes substantially more exothermic with increasing SWCNT diameter. Admittedly, the largest barrier (I-TS) relative to I-R (for the (4,4) SWCNT, Figure 6b) exhibits a $\Delta G^{\ddagger}$(500 K) value of only *ca.* 6.7 kcal/mol, and so such a reaction is extremely favorable. Interestingly, $\Delta G^{\ddagger}$(500 K) corresponding to pentagon defect formation (Figure 6b) is consistently lower for all SWCNT diameters. Recalling that 1 $kT \approx 1$ kcal/mol at 500 K, defect formation *via* this process is effectively barrierless for any SWCNT with a diameter larger than that of a (10,10) SWCNT. Nevertheless, ΔG for the isomerization itself is significantly more favorable for hexagon formation (by *ca.* 20 kcal/mol for all [*n*]CPP). These processes are therefore expected to be highly competitive during SWCNT growth; this is indeed the case according to Figure 5.

4.3. C_2H Insertion versus DA-Cycloaddition: Dependence on Diameter. The decomposition of acetylene, forming C_2H, has been established on a variety of substrates/catalysts at low temperatures.[37,38] In reality however, the C_2H radical is anticipated to be present only in trace quantities in experimental CVD growth conditions. In the current context, the possibility of SWCNT growth *via* DA cycloaddition therefore cannot be overlooked; nor can C_2H_2 addition to dehydrogenated organic precursors. The energetics of such processes is presented in Figure 7. Here we limit our discussion to (*n*,*n*) armchair SWCNTs, based on the similarities between hexagon addition for all (*n*,*m*) SWCNTs (i.e., all addition takes place at an edge armchair structure).

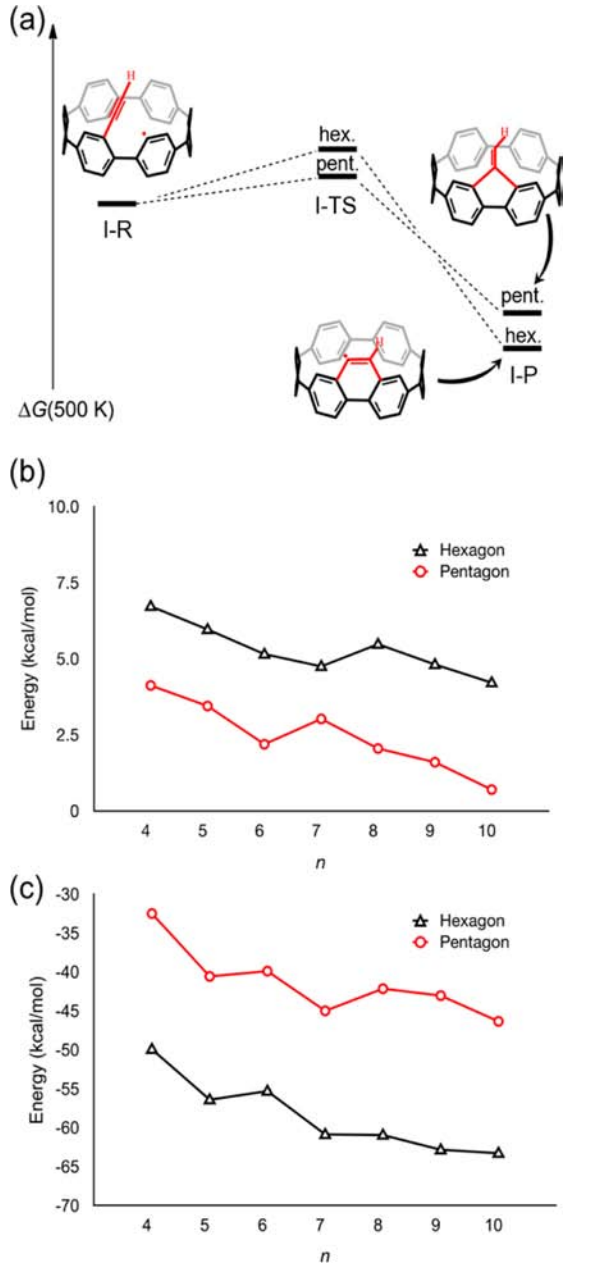

Figure 6. (a) Reaction mechanism for hexagon/pentagon addition to [*n*]CPP precursors following C_2H insertion (I-R). (b) $\Delta G^{\ddagger}$(I-TS) and (c) ΔG(I−P), relative to I-R, for hexagon/pentagon addition to [*n*]CPP precursors. All data were computed using B3LYP/6-31G(d); Gibbs free energies were calculated at 500 K.

Comparison between Figure 6 and Figure 7 immediately illustrates how labile SWCNT growth *via* the C_2H insertion mechanism is, compared with that based on DA cycloaddition. For [*n*]CPPs (n = 4−10), all of which have the same chiral angle θ (30°), barriers for C_2H insertion range between 4.2−6.7 kcal/mol (I-TS). On the other hand, barriers for DA cycloaddition to [*n*]CPP range between 64−69 and 68−79 kcal/mol (II-TS1) for *endo* and *exo* C_2H_2 addition, respectively (Figure 7). The barriers of the two growth mechanisms therefore differ roughly by an order of magnitude. It is obvious that for an equivalent C_2H/C_2H_2 feedstock ratio, the C_2H

dx.doi.org/10.1021/ja305769v | J. Am. Chem. Soc. 2012, 134, 15887−15896

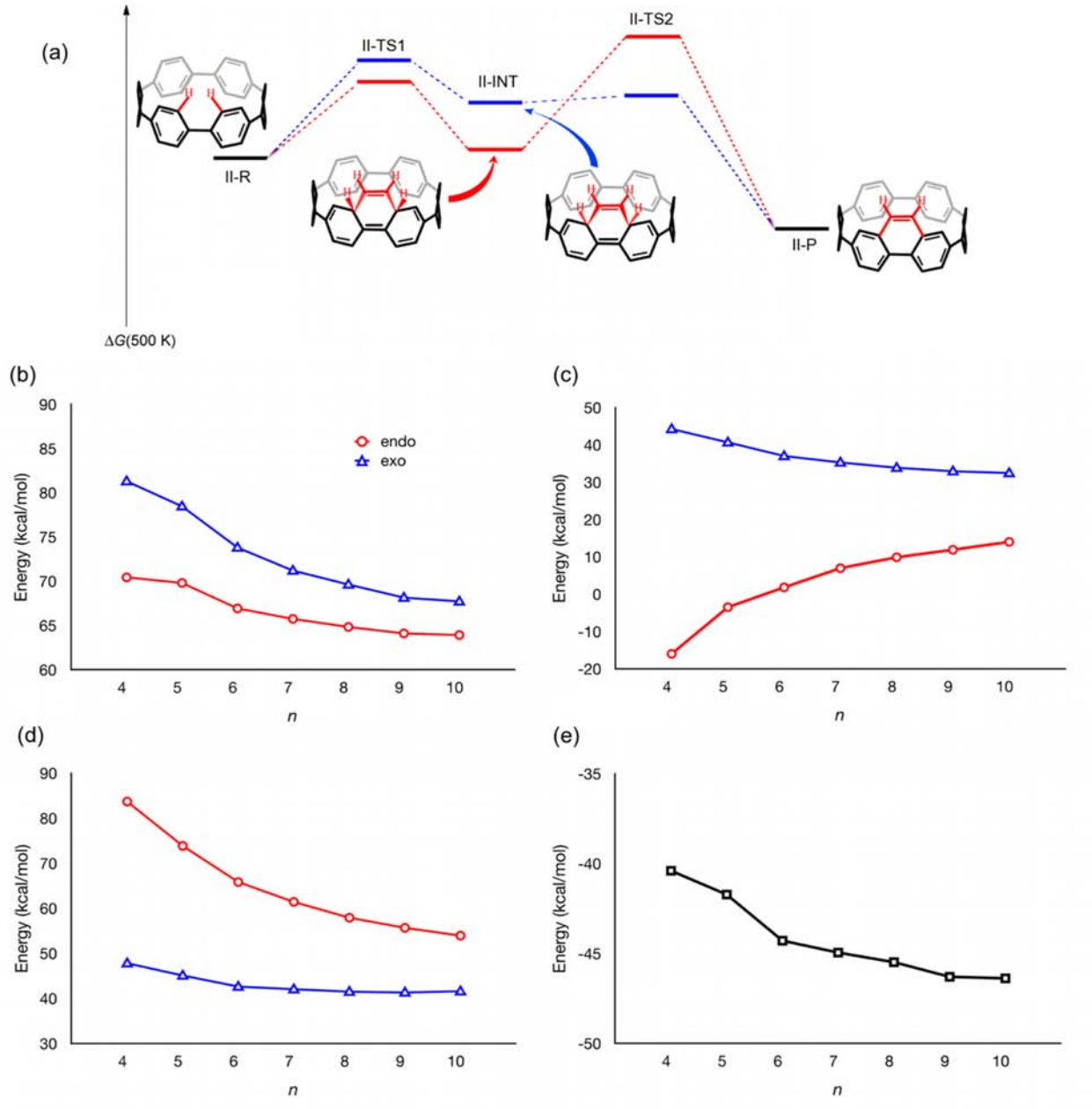

Figure 7. (a) Reaction mechanism for hexagon addition to [*n*]CPP precursors (II-R) and H_2 renormalization *via* DA cycloaddition. (b) $\Delta G^{\ddagger}$(II-TS1), (c) ΔG(II-INT), (d) $\Delta G^{\ddagger}$(II-TS2), and (e) ΔG(II−P), relative to II-R, for [*n*]CPP precursors. All data computed using B3LYP/6-31G(d); Gibbs free energies calculated at 500 K.

radical insertion mechanism will dominate the kinetics of SWCNT growth rate, instead of the DA cycloaddition mechanism. However, this dominance of C_2H radical insertion is negated by the trace amounts at which C_2H radicals are expected to be present in experimental growth conditions. Thus, the role of C_2H_2 DA cycloaddition on SWCNT growth cannot be ruled out completely due to thermodynamic considerations, particularly at high temperature. We note here that *exo* addition typically yields asymmetrical II-TS1 structures; nevertheless C_2H_2 insertion only involves a single TS despite previous assumptions to the contrary.[28] More importantly, while SWCNT growth *via* C_2H radical addition leads to diameter-independent growth rates, Figure 7 indicates that the opposite is the case regarding DA-based SWCNT growth. In particular, $\Delta G^{\ddagger}$(500 K) for C_2H_2 cycloaddition (II-TS1) is inversely proportional to the SWCNT diameter, indicating more labile SWCNT growth for larger-diameter SWCNTs. These findings are consistent with experimentally reported abundances of near-armchair SWCNTs.[16] In such a scenario diameter-independent theories of SWCNT growth[40] are therefore no longer applicable. We are assuming here that no prior H-abstraction from the organic precursor has taken place. In such a case, chirality-controlled SWCNT growth necessitates H_2 renormalization (the removal of two H atoms from the two sp^3 carbons regaining π−conjugation) following C_2H_2 cycloaddition, otherwise defective sp^3-hybridized carbon atoms remain in the growing SWCNT. Figure 7 shows that this is the rate-limiting step of the entire DA-based growth process, and is one that exhibits a strong dependence on SWCNT diameter; $\Delta G^{\ddagger}$(500 K) ranges between 42−48 (*exo*) and 54−

dx.doi.org/10.1021/ja305769v | J. Am. Chem. Soc. 2012, 134, 15887−15896

83 (*endo*) kcal/mol (II-TS2). Once again, the height of this barrier is inversely proportional to SWCNT diameter; in the case of *endo* addition, the trend is most notably pronounced. Interestingly, while *endo* C_2H_2 cycloaddition is more favorable than *exo* cycloaddition (II-INT), the opposite is the case for H_2 renormalization. Hexagon addition *via* DA cycloaddition is ultimately strongly exothermic, with ΔG ranging from −40 to −46 kcal/mol. However, while the intermediate II-INT in the case of *exo* addition is always highly endothermic (32−44 kcal/mol), this is not the case for *endo* addition. Instead, the latter is exothermic for small SWCNT diameters and becomes endothermic for larger SWCNT diameters. Ironically, however, H_2 renormalization for these smaller diameter, more stable II-INT species correspond to the highest barriers.

In the case where the organic precursor is dehydrogenated prior to interaction with acetylene, the hexagon formation mechanism itself no longer resembles a DA process; instead C_2H_2 insertion takes place *via* a metastable intermediate structure.[36] Further details of this process are provided as Supporting Information (Figure S2), suffice to note here the following points. First, C_2H_2 addition following CPP hydrogen abstraction is a significantly more favorable process, with $\Delta G^{\ddagger}$(500 K) no higher than 22.5 kcal/mol for any [*n*]CPP species. Second, and perhaps more importantly, the marked relationship between [*n*]CPP diameter and $\Delta G^{\ddagger}$(500 K) for C_2H_2 DA cycloaddition, discussed above, is no longer present for C_2H_2 addition to dehydrogenated [*n*]CPP precursors. In the case of DA cycloaddition, new C−C bonds are formed *via* $\pi-\pi$ orbital interactions between the SWCNT "bay" carbon atoms and those in the C_2H_2 dienophile. The energetics of such cycloaddition are therefore determined by the SWCNT/C_2H_2 orbital overlap, which in turn is determined by the curvature (or diameter) of the SWCNT edge. In the case of C_2H_2 addition to dehydrogenated [*n*]CPP precursors, new C−C bonds are formed *via* σ-radical interactions, and so the extent of $\pi-\pi$ orbital overlap becomes irrelevant. This gives rise to a diameter-independent SWCNT growth rate; a result that is consistent with QM/MD simulations of SWCNT growth *via* C_2H addition.

5. CONCLUSION

We have demonstrated catalyst-free, chirality-controlled growth of chiral and zigzag single-walled carbon nanotubes (SWCNTs) from organic precursors using quantum chemical simulations. Comparison of C_2H- and C_2H_2-based growth mechanisms highlights the role of the C_2H radical in the growth of chiral and zigzag SWCNTs, as well as the growth of armchair SWCNTs.[36] In agreement with current experimental and theoretical data concerning transition-metal catalyzed SWCNT growth, we have shown here that the SWCNT growth rate under significantly different (i.e., low temperature, catalyst-free) conditions correlates directly with the chiral angle θ of the SWCNT fragment. This relationship is therefore an intrinsic property of the SWCNT edge structure itself; the trend may presumably only be enhanced or minimized, but hardly reversed, by altering the conditions of growth. On the other hand, results presented here suggest that the relationship between the SWCNT's diameter and its rate of growth depends explicitly on the growth conditions. Contemporary theories of SWCNT growth rates,[40] which are shown to be in good agreement with experimental data,[15,56,61] are implicitly diameter-independent. Our simulations of C_2H-based SWCNT growth also show diameter-independent SWCNT growth rates. Conversely, the energetics of SWCNT growth *via* DA-based cycloaddition of C_2H_2 is influenced strongly by the SWCNT diameter, with the growth rate being proportional to the SWCNT diameter. Under such conditions, SWCNT diameter must therefore be taken into account if the mechanism and kinetics of SWCNT growth are to be understood. Most notably, our theoretical investigation points to the possibility that, for a given C_2H/C_2H_2 feedstock ratio, a SWCNT diameter/chirality combination that yields a maximum growth rate exists.

■ ASSOCIATED CONTENT

Supporting Information

Cartesian coordinates of [*n*]CPP precursors and their DFTB energies; details of C_2H_2 addition to [*n*]CPP radical precursors; snapshots of small diameter SWCNTs; QuickTime movies depicting the evolution of SWCNT growth; complete refs 19 and 54. This material is available free of charge via the Internet at http://pubs.acs.org.

■ AUTHOR INFORMATION

Corresponding Author

*sirle@chem.nagoya-u.ac.jp; keiji.morokuma@emory.edu

Author Contributions

†These authors contributed equally.

Notes

The authors declare no competing financial interest.

■ ACKNOWLEDGMENTS

This work was in part supported by a CREST (Core Research for Evolutional Science and Technology) grant in the Area of High Performance Computing for Multiscale and Multiphysics Phenomena from JST. A.J.P. acknowledges the Fukui Fellowship, Kyoto University. The authors are grateful for generous supercomputer time at the Institute for Molecular Science (IMS) in Okazaki, Japan.

■ REFERENCES

(1) Dresselhaus, M. S.; Dresselhaus, G.; Eklund, P. C. *Science of Fullerenes and Carbon Nanotubes*; Academic Press: San Diego, 1996.

(2) Saito, R.; Dresselhaus, M. S.; Dresselhaus, G. *Physical Properties of Carbon Nanotubes*; Imperial College Press: London, 1998.

(3) Baughman, R. A.; Zakhidov, A. A.; de Heer, W. A. *Science* **2002**, *297*, 787−792.

(4) Frank, S.; Poncharal, P.; Wang, Z. L.; Heer, W. A. *Science* **1998**, *280*, 1744−1746.

(5) Okawa, Y.; Aono, M. *Nature* **2001**, *409*, 683−684.

(6) Saito, R.; Fujita, M.; Dresselhaus, G.; Dresselhaus, M. S. *Phys. Rev. B* **1992**, *46*, 1804−1811.

(7) Bethune, D. S.; Kiang, C. H.; DeVries, M. S.; Gorman, G.; Savoy, R.; Beyers, R. *Nature* **1993**, *363*, 605−607.

(8) Iijima, S. *Nature* **1993**, *363*, 603−605.

(9) Journet, C.; Maser, W. K.; Bernier, P.; Loiseau, A.; Lamy de la Chapelle, M.; Lefrant, S.; Deniard, P.; Lee, R.; Fischer, J. E. *Nature* **1997**, *388*, 756−758.

(10) Guo, T.; Nikolaev, P.; Thess, A.; Colbert, D. T.; Smalley, R. E. *Chem. Phys. Lett.* **1995**, *243*, 49−54.

(11) Thess, A.; Lee, R.; Nikolaev, P.; Dai, H.; Petit, P.; Robert, J.; Xu, C.; Lee, Y. H.; Kim, S. G.; Rinzler, A. G.; Colbert, D. T.; Scuseria, G. E.; Tomanek, D.; Fischer, J. E.; Smalley, R. E. *Science* **1996**, *273*, 483−487.

(12) Cheng, H. M.; Li, F.; Sun, X.; Brown, S. D. M.; Pimenta, M. A.; Marucci, A.; Dresselhaus, G.; Dresselhaus, M. S. *Chem. Phys. Lett.* **1998**, *289*, 602−610.

(13) Nikolaev, P.; Bronikowski, M. J.; Bradley, R. K.; Rohmund, F.; Colbert, D. T.; Smith, K. A.; Smalley, R. E. *Chem. Phys. Lett.* **1999**, *313*, 91−97.
(14) Page, A. J.; Ohta, Y.; Irle, S.; Morokuma, K. *Acc. Chem. Res.* **2010**, *43*, 1375−1385.
(15) Bachilo, S. M.; Balzano, L.; Herrera, J. E.; Pompeo, F.; Resasco, D. E.; Weisman, R. B. *J. Am. Chem. Soc.* **2003**, *125*, 11186−11187.
(16) Wang, B.; Poa, C. H. P.; Wei, L.; Li, L.-J.; Yang, Y.; Chen, Y. *J. Am. Chem. Soc.* **2007**, *129*, 9014−9019.
(17) Ding, F.; Rosen, A.; Curtarolo, S.; Bolton, K. *Appl. Phys. Lett.* **2006**, *88*, 133110/1−133110/3.
(18) Moseler, M.; Cervantes-Sodi, F.; Hofmann, S.; Csanyi, G.; Ferrari, A. C. *ACS Nano* **2010**, *4*, 7587−7595.
(19) Hofmann, S.; et al. *Nano Lett.* **2007**, *7*, 602−608.
(20) Moors, M.; Amara, H.; de Bocarme, T. V.; Bichara, C.; Ducastelle, F.; Kruse, N.; Charlier, J. C. *ACS Nano* **2009**, *3*, 511−516.
(21) Hersam, M. C. *Nat. Nano* **2008**, *3*, 387−394.
(22) Omachi, H.; Segawa, Y.; Itami, K. *Acc. Chem. Res.* **2012**, *45*, 1378−1389.
(23) Bunz, U. H. F.; Menning, S.; Martín, N. *Angew. Chem., Int. Ed.* **2012**, *51*, 7094−7101.
(24) Schrettl, S.; Frauenrath, H. *Angew. Chem., Int. Ed.* **2012**, *51*, 6569−6571.
(25) Hitosugi, S.; Yamasaki, T.; Isobe, H. *J. Am. Chem. Soc.* **2012**, *134*, 12442−12445.
(26) Sisto, T. J.; Tian, X.; Jasti, R. *J. Org. Chem.* **2012**, *77*, 5857−5860.
(27) Fort, E. H.; Donovan, P. M.; Scott, L. T. *J. Am. Chem. Soc.* **2009**, *131*, 16006−16007.
(28) Fort, E. H.; Scott, L. T. *J. Mat. Chem.* **2011**, *21*, 1373−1381.
(29) Jasti, R.; Bhattacharjee, J.; Neaton, J. B.; Bertozzi, C. R. *J. Am. Chem. Soc.* **2008**, *130*, 17646−17647.
(30) Jasti, R.; Bertozzi, C. R. *Chem. Phys. Lett.* **2010**, *494*, 1−7.
(31) Yamago, S.; Watanabe, Y.; Iwamoto, T. *Angew. Chem.* **2010**, *122*, 769−771.
(32) Omachi, H.; Matsuura, S.; Segawa, Y.; Itami, K. *Angew. Chem., Int. Ed.* **2010**, *49*, 10202−10205.
(33) Omachi, H.; Segawa, Y.; Itami, K. *Org. Lett.* **2011**, *13*, 2480−2483.
(34) Scott, L. T.; Jackson, E. A.; Zhang, Q.; Steinberg, B. D.; Bancu, M.; Li, B. *J. Am. Chem. Soc.* **2011**, *134*, 107−110.
(35) Xia, J.; Jasti, R. *Angew. Chem., Int. Ed.* **2012**, *51*, 2474−2476.
(36) Li, H.-B.; Page, A. J.; Irle, S.; Morokuma, K. *ChemPhysChem* **2012**, *13*, 1479−1485.
(37) Rudenko, A. P.; Balandin, A. A.; Zabalotnaya, M. M. *Russ. Chem. Bull.* **1961**, *10*, 916−921.
(38) Hung, W.-H.; Bernasek, S. L. *Surf. Sci.* **1995**, *339*, 272−290.
(39) Wang, Y.; Gao, X.; Qian, H.-J.; Ohta, Y.; Wu, X.; Eres, G.; Morokuma, K.; Irle, S. *J. Am. Chem. Soc.* **2012**, Submitted.
(40) Ding, F.; Harutyunyan, A. R.; Yakobson, B. I. *Proc. Natl. Acad. Sci. U.S.A.* **2009**, *106*, 2506−2509.
(41) Ohta, Y.; Okamoto, Y.; Irle, S.; Morokuma, K. *J. Phys. Chem. C* **2009**, *113*, 159−169.
(42) Ohta, Y.; Okamoto, Y.; Page, A. J.; Irle, S.; Morokuma, K. *ACS Nano* **2009**, *3*, 3413−3420.
(43) Voter, A. F. *Phys. Rev. B* **1998**, *57*, R13985−R13988.
(44) Fedorov, A. S.; Fedorov, D. A.; Kuzubov, A. A.; Avramov, P. V.; Nishimura, Y.; Irle, S.; Witek, H. A. *Phys. Rev. Lett.* **2011**, *107*, 175506.
(45) Elstner, M.; Porezag, D.; Jungnickel, G.; Elsner, J.; Haugk, M.; Frauenheim, T.; Suhai, S.; Seifert, G. *Phys. Rev. B* **1998**, *58*, 7260−7268.
(46) Elstner, M. *Theor. Chem. Acc.* **2006**, *116*, 316−325.
(47) Saha, B.; Shindo, S.; Irle, S.; Morokuma, K. *ACS Nano* **2009**, *3*, 2241−2257.
(48) Weinert, M.; Davenport, J. W. *Phys. Rev. B* **1992**, *45*, 13709−13712.
(49) Wentzcovitch, R. M.; Martins, J. L.; Allen, P. B. *Phys. Rev. B* **1992**, *45*, 11372.
(50) Swope, W. C.; Andersen, H. C.; Berens, P. H.; Wilson, K. R. *J. Chem. Phys.* **1982**, *76*, 637−649.
(51) Martyna, G. J.; Klein, M. L.; Tuckerman, M. *J. Chem. Phys.* **1992**, *97*, 2635−2643.
(52) Becke, A. D. *J. Chem. Phys.* **1993**, *98*, 5648−5652.
(53) Lee, C. Y.; Yang, W.; Parr, R. G. *Phys. Rev. B* **1988**, *37*, 785−789.
(54) Frisch, M. J.; et al. *Gaussian 09*, Revision A.1; Gaussian Inc.: Wallingford, CT, 2009.
(55) Fukui, K. *Acc. Chem. Res.* **1981**, *14*, 363−368.
(56) Miyauchi, Y.; Chiashi, S.; Murakami, Y.; Hayashida, Y.; Maruyama, S. *Chem. Phys. Lett.* **2004**, *387*, 198−203.
(57) Liu, Y.; Dobrinsky, A.; Yakobson, B. I. *Phys. Rev. Lett.* **2010**, *105*, 235502/1−4.
(58) Reich, S.; Li, L.; Roberson, J. *Chem. Phys. Lett.* **2006**, *421*, 469−472.
(59) Kim, J.; Page, A. J.; Irle, S.; Morokuma, K. *J. Am. Chem. Soc.* **2012**, *134*, 9311−9319.
(60) Peng, L. M.; Zhang, Z. L.; Xue, Z. Q.; Wu, Q. D.; Gu, Z. N.; Pettifor, D. G. *Phys. Rev. Lett.* **2000**, *85*, 3249−3252.
(61) Rao, R.; Liptak, D.; Cherukuri, T.; Yakobson, B. I.; Maruyama, B. *Nat. Mater.* **2012**, *11*, 213−216.